Can Satellite Observations offer a Water Cycle Model-Diagnostic for the MJO

D. Waliser, B. Tian , M. Schwartz, X. Xie, W. T. Liu, E. Fetzer
Jet Propulsion Laboratory, California Institute of Technology, Pasadena, California

Abstract

Many characterizations of the Madden-Julian Oscillation (MJO) have focused on its convection and circulation features, ocean interactions, and weather and climate impacts. The water cycle of the MJO offers an additional constraint on model representations of the MJO. Recent satellite products now make it possible to characterize the MJO water cycle from observations. These include water vapor profiles, column water vapor, cloud ice profiles, total cloud liquid, rainfall, surface evaporation and column moisture convergence. From these, we quantify the water budget for disturbed and suppressed phases of the MJO. The column-integrated results indicate that precipitation is nearly balanced with moisture convergence, with variations in surface evaporation being an order of magnitude smaller. However, residuals in the column-integrated budget are relatively large, indicating the need for improved satellite retrievals and/or the necessity of using model-based assimilation products.

1. Data Sets

- CMAP Rainfall : global, 2.5°x2.5° lat-long, pentad, 01/01/1979-02/22/2007. Xie and Arkin (1997)
- TRMM 3B42 Rainfall: 40S-40N, 0.25° x 0.25°, 3-hourly, 01/01/1998-06/30/2007. Huffman et al. (2007)
- AIRS H2OVapMMR & TotH2OVap V4, L3, global, 1.0° x 1.0°, 2Xdaily, 09/01/2002-04/30/2007. Chahine et al. (2006)
- QuikSCAT & TMI Moisture Transport 40S-40N, 0.25° x 0.25°, 2Xdaily, 08/1999-12/31/2005. Liu and Tang (2005)
- OAFlux Evaporation 65S-65N, 1.0° x 1.0°, daily, 01/01/1981-12/31/2002. Yu and Weller (2007)
- SSMI Total Column H2O Vapor & Total Cloud Liquid H2O V6, DMSP F13, global, 0.25° x 0.25°, 2Xdaily, 01/01/1996-06/30/2007. Wentz (1997), Wentz and Spencer (1998)
- MLS Ice Water Content 80S-80N, 4° x 8° lat-long, 2Xdaily, 08/26/2004-02/22/2007. Wu et al. (2006)

2. MJO Event Selection

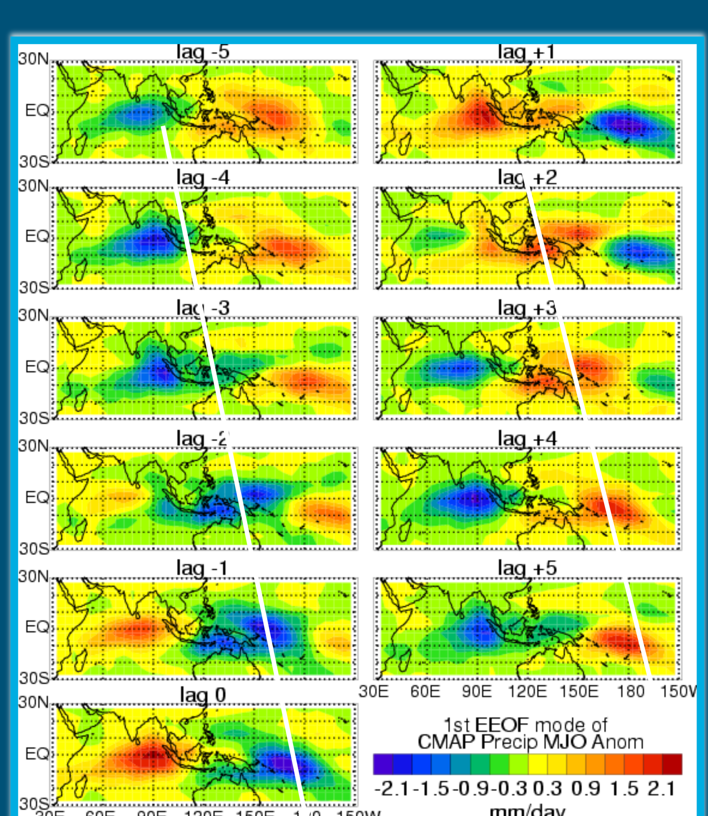

The selection of MJO events is based on computing an extended EOF (EEOF; left) from intraseasonally bandpassed rainfall and selecting the high amplitude (> 1) events from the EEOF time series (below). This provides 11-pentad composites of the MJO. In this case, the number of events for each variable's composite is dependent on the record length and period (given below).

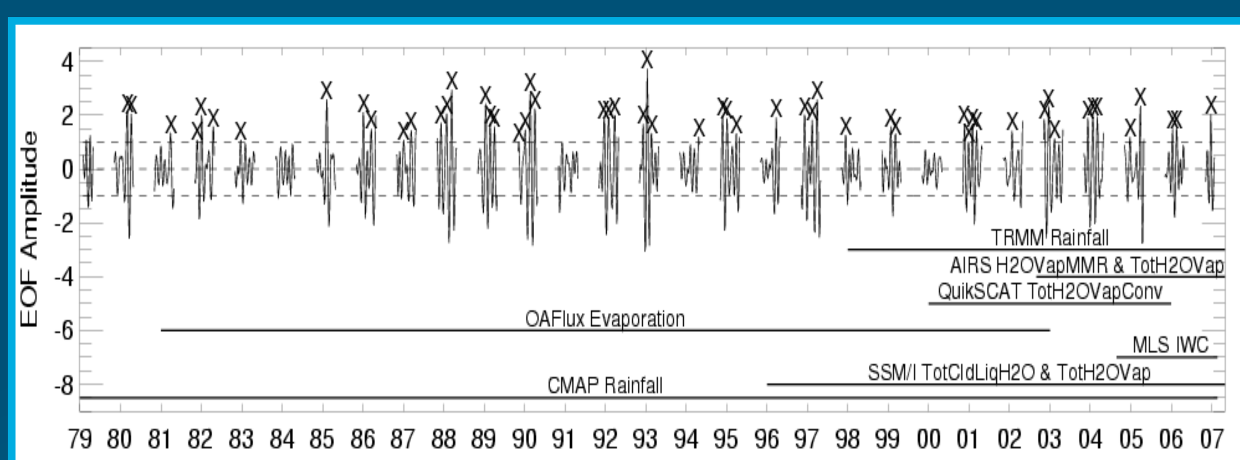

3. Rainfall Pattern & Data Sensitivity

The figures below show the rainfall and water vapor patterns over a selected number of pentad lags of the composite MJO. The two figures on the left compare the two rainfall data sets used in this analysis and their sensitivity to the data period. The figure on the right shows similar information for the column water vapor. Overall, for the choice of data sets shown here, the data period does not have too much impact on the qualitative aspect of the composite.

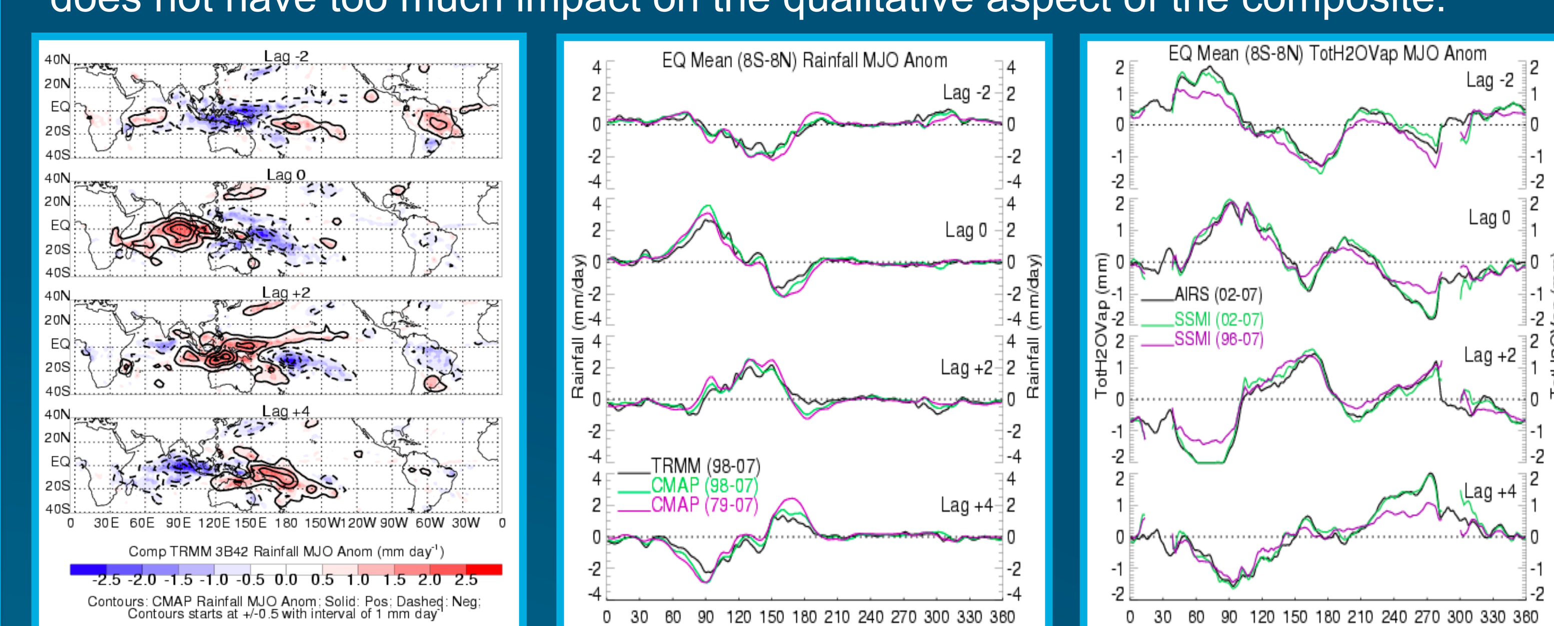

4. Some Composite Results

Rainfall and total column moisture convergence tend to be correlated throughout Tropics (left panel), with precipitation modestly lagging total column moisture convergence in some regions/lags. The largest evaporation anomalies (middle panel) are in the subtropics and occur in association with Rossby gyre modulations of the trade wind regimes. The near-equatorial evaporation anomalies are small and tend to lag precipitation anomalies. Vertical structure information from AIRS water vapor (see also Tian et al. 2006, 2010) and MLS cloud ice in the upper troposphere (see also Schwartz et al. 2008) is given in the right panel along with other near-equatorial averaged quantities.

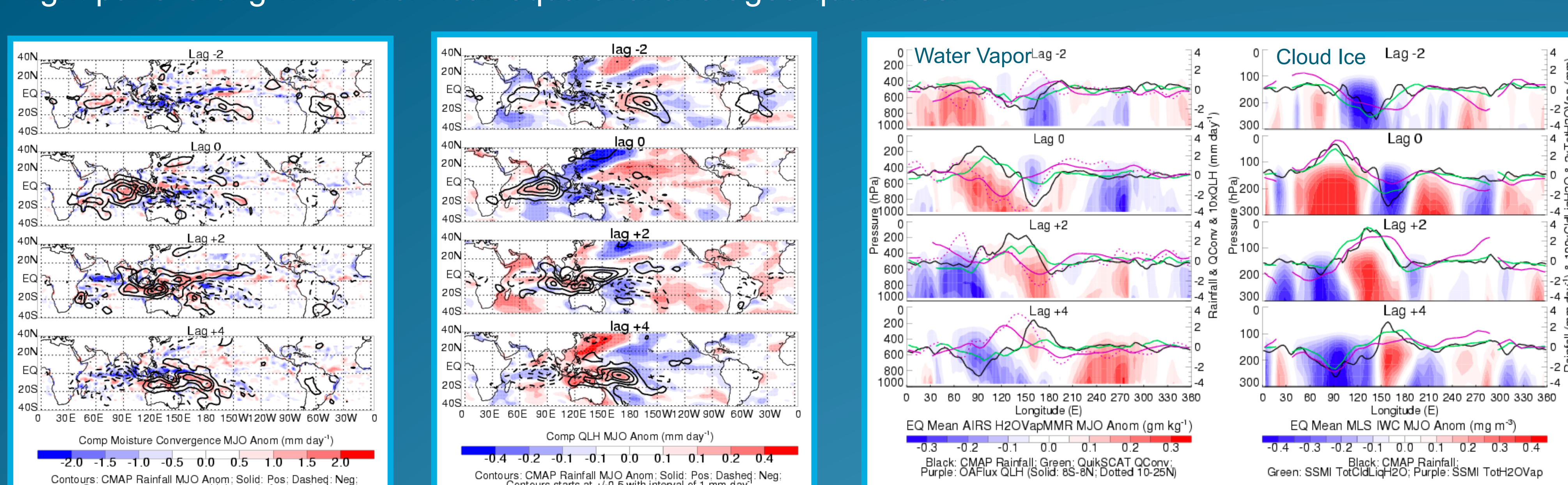

5. Integrated Findings

The two schematics below provide an overview of the composite MJO Water Cycle based on contemporary satellite data. The upper panel is taken from our companion study on the upper-troposphere lower-stratosphere using MLS data (Schwartz et al. 2007). The lower diagram is based on the results discussed here. The panel on the left illustrates the magnitudes and longitudinal structure of the water cycle terms for the near-equatorial region. Evident is the near balance between precipitation and total column moisture convergence – and the slight lag between the two - with other terms being considerably smaller. Of concern is that the residual is of the same order of magnitude as the two dominant terms.

$$\partial W / \partial t + P - MC - E = residual$$

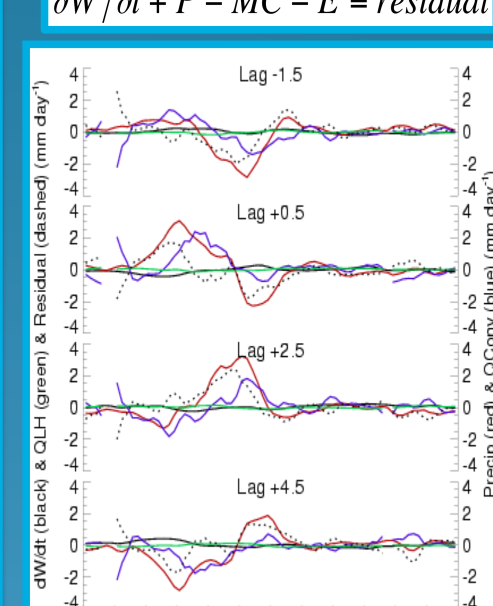

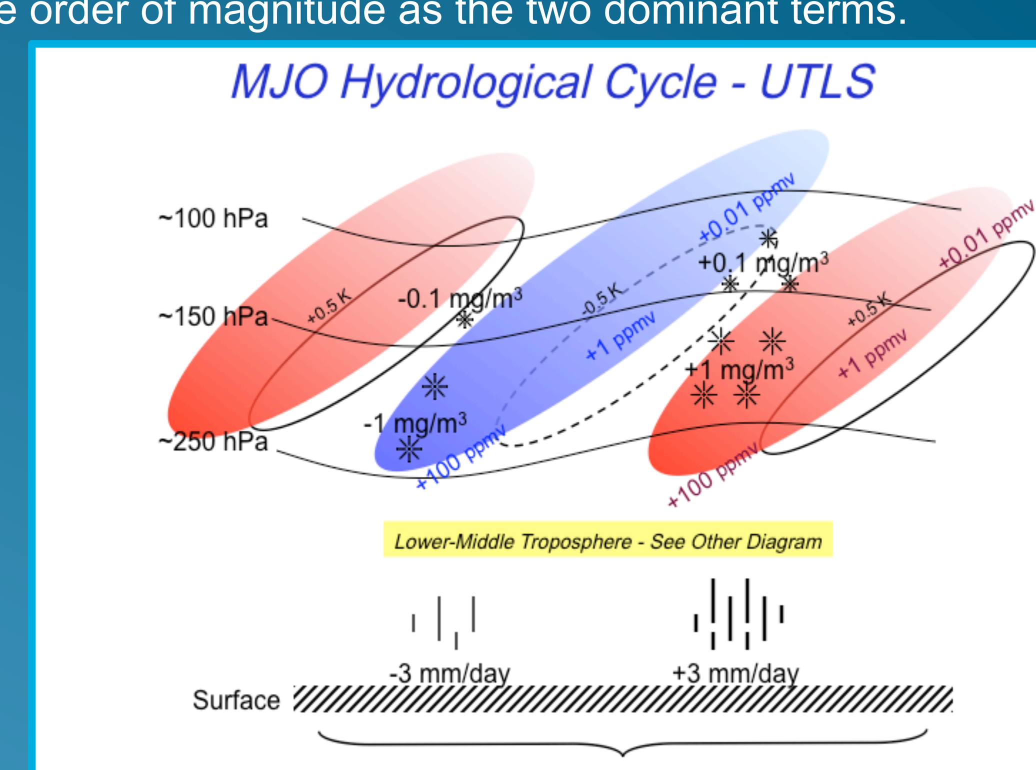

Upper Schematic Caption:. **MJO equatorial (10N–10S) hydrological structure schematic. H2O anomalies are** shaded pink/blue and temperature anomalies are solid/dashed lines, positive/negative respectively. The magnitudes of IWC anomalies are indicated by the density of snowflake symbols.

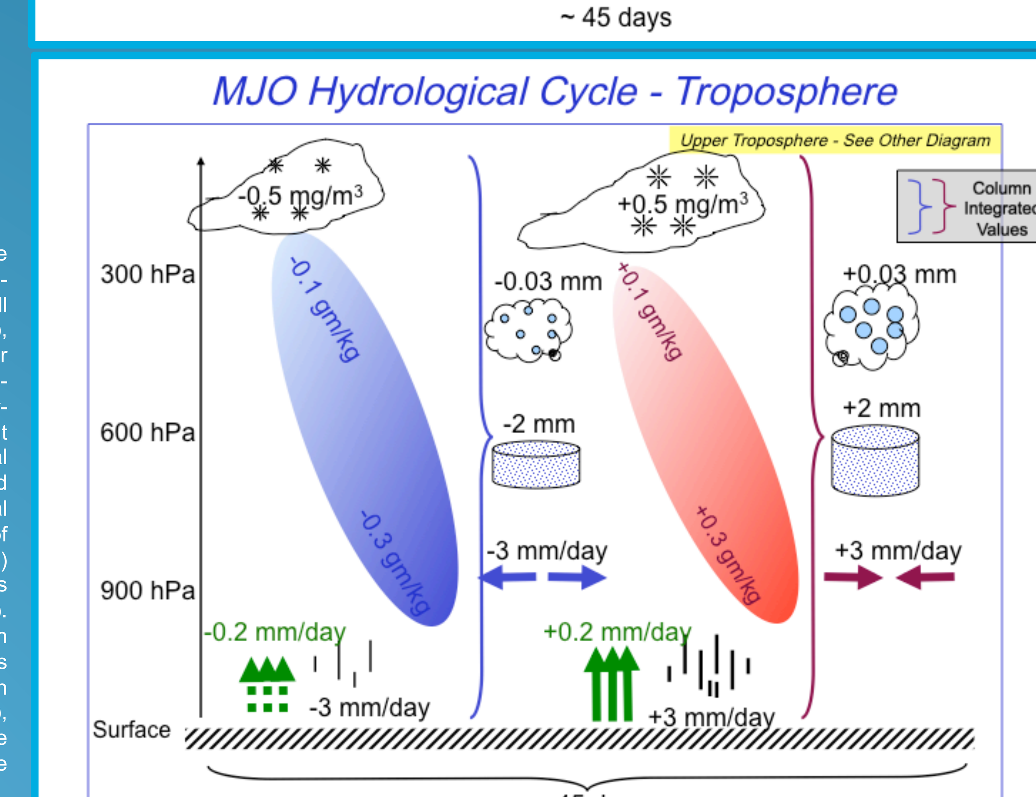

Lower Schematic Caption: (a) Pressure-longitude cross-sections of composite near-equatorial (8°S - 8°N) anomalies of water vapor (gm kg-1), rainfall (mm day-1), moisture convergence (mm day-1), surface evaporation (0.1 mm day-1), and the latter using the latitude range 10-25oN. (b) Pressure-longitude cross-sections of composite near-equatorial (8°S - 8°N) anomalies of ice water content (mg m-3), CMAP rainfall (mm day-1), SSM/I total precipitable water (0.5 mm), and total cloud liquid water (0.01 mm). (c) Schematic of the hydrological cycle associated with the MJO. Left (right) half of diagram is associated with subsidence (convective) phase of the MJO. Green dashed (black solid) lines near surface represent evaporation (precipitation). Blue (red) oval represents water vapor anomalies in subsidence (convective) phase of the MJO. Items next to blue (red) brackets indicate column integrated liquid water (cloud with small circles), water vapor (cylinder) and moisture convergence (horizontal arrows). Clouds with asterisks indicate upper tropospheric cloud ice.

References

Chahine, M. T., et al. (2006), Improving weather forecasting and providing new data on greenhouse gases, Bull. Amer. Meteor. Soc., 87(7), 911-+.
Huffman, G. J., et al. (2007), The TRMM Multisatellite Precipitation Analysis (TMPA): Quasi-Global, Multiyear, Combined-Sensor Precipitation Estimates at Fine Scales, J. HydroMet., 8(1), 38-55.
Liu, W. T., and W. Q. Tang (2005), Estimating moisture transport over oceans using space-based observations, J. Geoph. Res. - Atmos., 110(D10).
Schwartz, M. J., et al. (2007), MJO in EOS MLS cloud ice and water vapor., Geophys. Res. Lett., 35, L08812, doi:10.1029/2008GL033675.
Tian, B., et al. (2006), Vertical moist thermodynamic structure and spatial-temporal evolution of the MJO in AIRS observations, Journal of the Atmospheric Sciences, 63(10), 2462-2485.
Tian, B., D. E. Waliser, E. J. Fetzer, and Y. L. Yung (2010), Vertical moist thermodynamic structure of the Madden-Julian Oscillation in Atmospheric Infrared Sounder retrievals: An update and a comparison to ECMWF reanalysis. Mon. Wea. Rev., In Press.
Wentz, F. J. (1997), A well-calibrated ocean algorithm for special sensor microwave/imager, J. Geoph. Res. - Oceans, 102(C4), 8703-8718.
Wentz, F. J., and R. W. Spencer (1998), SSM/I rain retrievals within a unified all-weather ocean algorithm, Journal of the Atmospheric Sciences, 55 (9), 1613-1627.
Wu, D. L., et al. (2006), EOS MLS cloud ice measurements and cloudy-sky radiative transfer model, EEE GRS Aura Special Issue, 44(5), 1156-1165.
Xie, P. P., and P. A. Arkin (1997), Global precipitation: A 17-year monthly analysis based on gauge observations, satellite estimates, and numerical model outputs, Bull. Amer. Meteor. Soc., 78(11), 2539-2558.
Xie, P. P., et al. (2003), GPCP Pentad precipitation analyses: An experimental dataset based on gauge observations and satellite estimates, J. Clim., 16(13), 2197-2214.
Xie, X. S., et al. (2008), Spacebased estimation of moisture transport in marine atmosphere using support vector regression, Remote Sens. Environ., 112(4), 1846-1855.
Yu, L. S., and R. A. Weller (2007), Objectively analyzed air-sea heat fluxes for the global ice-free oceans (1981-2005), Bull. Amer. Meteor. Soc., 88 (4), 527-539.